Journal of Thermal Spray Technology, Volume 20, Number 4, 2011, Pages 909-917

Corrosion performance of laser post-treated cold sprayed titanium coatings

T. Marrocco, T. Hussain, D.G. McCartney and P.H. Shipway

The recent development of cold spray technology has made possible the deposition of highly reactive, oxygen sensitive materials, such as titanium, without significant chemical reaction of the powder, modification of particle microstructure and with minimal heating of the substrate. However, the presence of interconnected pathways (micro-scale porosity) within the deposit limits the performance of the metallic coating as an effective barrier to corrosion and substrate attack by corrosive media is usually inevitable. The aim of the present study was to investigate the effects of processing, including a post-spray laser treatment, on the deposit microstructure and corrosion behavior. Commercially pure titanium (CP Ti) was deposited onto a carbon steel substrate, using a commercial cold spray system (CGT^{TM} Kinetiks® 4000) with pre-heated nitrogen as both the main process gas and the powder carrier gas. Selected coatings were given a surface melting treatment using a commercial 2kW CO_2 laser (505 Trumpf DMD). The effect of post-deposition laser treatment on corrosion behavior was analyzed in terms of pore structure evolution and microstructural changes. Optical microscopy, scanning electron microscopy and X-ray diffraction were employed to examine the microstructural characteristics of the coatings. Their corrosion performance was investigated using electrochemical methods in 3.5wt.% NaCl (ASTM G5-94(2004)). As-sprayed titanium coatings could not provide favorable protection to the carbon steel substrate in the aerated NaCl solution whereas the coatings with laser-treated surfaces provided barrier-like properties.

Keywords: cold spray, titanium, corrosion, laser treatment.

1 Introduction

Thanks to their many unique characteristics, titanium and its alloys perform very well (as few other materials can) in many challenging environments, such as aerospace, petrochemical, marine, bio-implants and motorsports [1]. The outstanding resistance to corrosion in a wide range of aggressive media is a result of a tenacious protective oxide layer (TiO_2), which is always present because of the high affinity of titanium for oxygen and water vapor. The oxide film is sufficiently thick to passivate the metal and is quickly re-established when locally destroyed, e.g. by mechanical action [2]. With the high price of corrosion resistant materials (such as titanium and its alloys) in bulk form, there are major financial incentives to use Ti-coated, lower cost substrates. Increasing attention has been paid to the spraying of titanium with the deposited coatings designed to be used for protection of substrates, particularly, in aqueous environments where electrochemical corrosion can occur [3].

Thermal spraying (typically flame or plasma spraying) of reactive materials such as titanium can cause a considerable change in chemical composition from powder to coating, which should be minimized as far as possible. During spraying, gas adsorption onto particles from the atmosphere, decomposition, phase changes and oxidation or nitridation of the spray particles can occur in ways that may be difficult to control [4]. Additionally, oxidation of spray particles after impact is also potentially significant due to their exposure to the atmosphere with an increased surface area produced by deformation (flattening) whilst still hot and during the cooling period. In some applications (e.g. biotechnology), phase purity is of utmost importance, and oxidation or phase changes that occur during the spray operation can lead to total rejection of the sprayed coating. If interactions between the molten particles and the reactive gas molecules are detrimental to the properties and the particular application, spraying in a vacuum chamber has been, hitherto, the main alternative [5].

On the other hand, cold spray, as a solid-state process, permits deposition of titanium coatings under open atmospheric conditions without significant reaction (with oxygen or nitrogen) and with generally low porosity. The process involves the acceleration of fine powders to 500-1000$m.s^{-1}$ in a supersonic inert gas jet. On impact with the target surface, the solid particles experience high strain rate deformation, forming a bond with the substrate and each other to produce a low porosity and well adhered coating [6]. The technology has now reached a significant stage in its industrialization, with

proven commercial equipment now available, together with suppliers offering specially developed powders to ensure good coating quality. Specifically, absence of porosity in cold sprayed titanium coatings plays a critical role in forming a corrosion resistant barrier layer. The type of gas used as the main process gas has a strong influence on the porosity of the coatings [7-9]. Generally, a less porous coating structure has been observed when helium is used as the accelerating gas (compared to coatings sprayed with nitrogen) because the particle velocity is greatly increased under the same operating conditions due to the higher specific heat and lower molecular weight of helium [10]. Evidence of this can be found in the study carried out by Li and Li [11], which reveals formation of large pores open to the surface when titanium coatings were cold sprayed using nitrogen as the propellant gas.

Hence attack of substrates which are not corrosion resistant by corrosive media is usually inevitable as reported in detail by the present authors in reference [12]. In reference [12] it is shown that deposits sprayed with heated nitrogen gas onto carbon steel substrates could be produced with a total interconnected porosity of 5.9vol.% such that 4.5vol% was below 1µm with the balance above 1µm in size. These measurements were obtained using mercury intrusion porosimetry. It was also shown [12] that these deposits did not provide an impermeable barrier. The corrosion performance of titanium (cold sprayed onto carbon steel substrate and bulk titanium) in natural seawater was also studied by Wang et al. [13] by using open circuit potential measurements and potentiodynamic polarization. They reported that the open circuit potential of cold sprayed titanium was more negative than the bulk titanium due to the high surface activity (of the top layer of the deposit) and limited bonding at the inter-particle boundaries. Similarly arc, flame, atmospheric plasma sprayed (shrouded) and warm sprayed titanium coatings show a higher corrosion current density compared to bulk titanium due to the presence of oxides, nitrides and most importantly porosity [14-17].

Laser processing is used in surface engineering for melting, cladding, alloying and transformation hardening of materials [18]. Typically, the very high power density of laser beam (~$10^{10\text{-}12}$W.m^{-2}) provides deep penetration. However, in the case of surface engineering applications, the beam is usually defocused to reduce penetration and increase coverage rate (i.e. it is possible to melt the coating while the substrate can remain virtually unaffected). In laser surface melting, the heat energy

from the laser beam is sufficient to melt the surface without vaporizing the material. A melt pool is formed at the material surface which is governed by the forces of buoyancy due to density difference and convection due to surface tension gradients. The bulk material acts as a heat sink and as soon as the laser beam traverses past, the solidification process starts from the solid-liquid interface towards the surface [19]. Laser melting of the coating promotes a homogeneous and refined microstructure as a result of rapid melting and solidification which potentially can improve corrosion properties. A number of post-spray treatments (e.g. laser surface melting and electron beam diffusion) have been reported to improve the corrosion behavior of plasma sprayed titanium coatings [1, 16, 20]. The laser-consolidated coating showed no evidence of corrosion after testing for 15 days whereas the coating left in the as-sprayed condition showed pitting corrosion of the steel at the coating-steel substrate interface [20].

The current study investigated the effects of a post-spray laser treatment performed on titanium coatings that were cold sprayed onto a carbon steel substrate. The microstructural characterization and porosity measurements (using mercury intrusion porosimetry) of the cold sprayed titanium coatings are extensively detailed in a previous publication by the authors [12]. In the present study, selected coatings from that original work were given a surface melting treatment using a 2kW Trumpf DMD 505 CO_2 laser and their microstructure and corrosion behavior investigated. Optical microscopy, scanning electron microscopy and X-ray diffraction were employed to examine the microstructural characteristics of the coatings. Their corrosion performance was investigated using electrochemical methods in 3.5wt% NaCl (ASTM G5-94(2004)).

2 Experimental Methods

2.1 Materials

Commercially pure gas-atomized titanium powder (LPW, Cheshire, UK) was used to produce the deposits. Details of the chemistry and nominal particle size distribution, as provided by the powder manufacturer, are reported in Table 1. The feedstock powder was spherical in shape with only a very small fraction exhibiting satellite particles, as expected for gas atomized powders (Fig.1a). The particle size distribution of the feedstock powder was measured using laser diffractometry (Table 1).

The particle size analysis measured by laser diffractometry showed that 90% of the particles were in the supplier specified size range of -30+10µm with approximately 10vol% below 10µm (Fig.1b).

All coatings were deposited onto grit-blasted carbon steel (BS 970-1:1983 Grade 045M10) substrates of dimension 40×25×2mm. All substrates were ultrasonically cleaned in acetone prior to use and given a final clean using acetone to remove any surface residue introduced whilst mounting the samples for spraying.

2.2 Spraying procedure

All coatings were deposited at TWI using a CGT Kinetiks 4000/47® cold spray system. The system is capable of spraying at gas pressures and temperatures of 40bar and 800°C, respectively. The spray gun was mounted on a 6-axis robot to allow accurate control of the spraying pattern and used with a de Laval nozzle with an area expansion ratio of ~6.5. In all cases, the coatings were deposited using oxygen-free nitrogen (OFN = <5ppm O_2, <8ppm H_2O) as both the main process and carrier gas. The main spray parameters used are shown in Table 2. Scanning the spraying gun over the coupons for a total of three passes, a coating thickness of ~500-600µm was achieved.

2.3 Post-spray laser treatment

Following coating deposition, samples were laser-treated using a Trumpf DMD 505 (Trumpf GmbH, Ditzingen, Germany) 2kW CO_2 laser. The laser was used to melt only the top layer of the material in a protective helium atmosphere to prevent, as far as possible, oxidation of titanium. The samples were clamped on a copper block to dissipate the heat produced from the laser heating and avoid distortion of the substrates and coatings and the possibility of delamination. The trials were carried out with laser power ranging from 440 to 1000W, a traverse speed of 21.6 to 48.3mm.s^{-1} and a beam diameter of 0.3 to 1.08 mm measured using a Prometec beam profiler (Prometec GmbH, Aachen, Germany).

A rectangular laser treated area (16×16mm) was prepared on each of the cold sprayed titanium coatings (40×25mm), using overlapping tracks. A number of preliminary trials were conducted to assess the appropriate conditions to achieve surface melting without delamination and study the shape and depth of melt pool. Five different laser process conditions were employed, as listed in

Table 3; Run 3 parameters were used to produce the laser treated areas that were subjected to corrosion testing

2.4 Microstructural characterization of coatings

A metallographic cross-section was prepared from each coating by cutting samples with a diamond slitting wheel. To remove any effects associated with cutting the specimen, following mounting, the sample was ground back ~2mm using P120 (125µm) grit silicon carbide (SiC) paper. Progressive grinding with finer grades was carried out, finishing with P1200 (15.3µm) grit SiC paper. This was followed by polishing with successively finer diamond pastes and then a final polishing using a 10:1 solution of suspended colloidal (0.1µm) silica solution and H_2O_2 on a MD-Chem cloth (Struers UK). The prepared sections were examined using optical and scanning electron microscopy. An FEI XL30 (FEI Europe, Eindhoven, The Netherlands) scanning electron microscope (SEM) operating at 20kV was employed to examine the microstructures of the coatings. The coatings were lightly etched in Kroll's etchant (2%HF, 5%HNO_3 and 95%H_2O) for a standard time of 15 seconds prior to examination in the microscope.

To determine the phases present in each coating both before and after laser treatment, X-ray diffraction was performed on the top surface using a Siemens D500 diffractometer (Siemens Analytics, Munich, Germany). This was operated at 40kV and 25mA to generate monochromatic Cu-K_α radiation with a wavelength of 0.15406nm. A 2θ diffraction angle ranging from 30° to 90° was employed with a dwell time of 5 seconds per step and a step size 0.05° Phases present in the spectra were identified with the aid of Joint Committee on Powder Diffraction Standards (JCPDS) diffraction files. Scans of the coatings were performed on 10 x10mm^2 samples mounted on a suitable holder.

2.5 Corrosion testing

To determine whether the titanium coating was resistant to chloride attack and whether it produced a physical barrier (i.e. no interconnected porosity) for the steel substrate, electrochemical studies were conducted on the coating in the as-sprayed and post-laser-treated conditions, using an ACM Gill 8 sequencer (ACM Instruments, Cumbria, UK). The samples were prepared to a P1200 (15.3µm) grit surface finish. The coatings were tested in a standard 3-electrode cell at 30 °C and in aerated 3.5wt%

NaCl aqueous solution. The open circuit potential (OCP) of the specimens was measured for the first 60 minutes of immersion before starting the potentiodynamic scans. To conduct the anodic scans, samples were first lowered to a potential 200mV below the open circuit value and then scanned in the anodic direction at a rate of 20mV.min^{-1}. All the potentials were measured with respect to an Ag/AgCl reference electrode and a platinum plate was used as a counter electrode.

Results

Initially, to allow the most suitable selection of parameters, the laser was scanned over the cold sprayed titanium coatings in a single pass and metallographic cross-sections were prepared from all the tracks to analyze the shape and depth of the melt pool as shown in the optical micrographs of Fig. 2. In all cases, the laser-treated regions are seen to comprise pore-free regions with equiaxed grains; making them easily distinguishable from the unmelted as-sprayed region featuring inter-particle porosity. The densification of the laser-treated region is due to its melting and porosity escaping to the free surface with the subsequent re-solidification of the treated area. An empirical relationship between power density parameters ($P/(DV)^{1/2}$, where P is the laser power, D the spot diameter and V the scanning traverse speed) and the melting depth was reported by Steen [18]. The relationship between this parameter and melted depth and width determined in the present study is shown in Table 3. From Run 3 to Run 5, the beam diameter was fixed at 1080µm and an increase of the $P/(DV)^{1/2}$ value correlates with a decrease of the melting depth. Increasing the power (P) increases the depth and width of the melted region by 20 and 100µm, respectively (Fig. 2 (a) and (b)) whereas, as the traverse speed (V) increases, the melted depth decreases but with less change in track width (Fig. 2 (c) to (e)). Values of depth and width of the melting regions are given in Table 3.

On the basis of these single tracks, Run 3, which had the highest $P/(DV)^{1/2}$ value, was selected to treat an area of 16×16mm. Overlapping track trials were performed using a range of track off-sets from 200 to 1000µm. Eventually, an off-set of 1000µm was used, resulting in a track overlap of only 200µm. The back- scattered electron (BSE) image of the etched cross-section of the laser treated coating is shown in Fig. 3 (a). Here, the depth of the laser melt pool can be identified as the point at which inter-particle pores of the titanium coating begin. It can be seen that, at the centre of the melt pool, the penetration depth is ~140µm whereas at the edge (i.e. where two laser tracks were

overlapped) is around ~100μm. Nevertheless, the parameters of Run 3 (Table 3) sealed the coating top surface uniformly and without any gaps. The high magnification, secondary electron (SE) image of the laser treated area (Fig. 3 (b)) reveals the acicular microstructure of titanium and isolated rounded pores (marked with arrows).

Figure 4 shows X-ray diffraction patterns of both the as-sprayed coating and the laser treated coating. Clearly, the main phase present in both cases is seen to be α-Ti. The pattern from the as-sprayed coating does not show any evidence for oxides or nitrides within the limits of XRD sensitivity (i.e., 1-2wt.%). However, for the laser treated coating, small peaks corresponding to TiO (Hongquiite) are seen at 2θ angles of 36°, 42° and 61°. This is evidence for some limited oxidation occurring during laser melting due to the high reactivity of titanium, despite the fact that the laser treatment was conducted in a protective helium atmosphere. The other feature of note is the evident peak broadening in the spectrum from the as-sprayed sample. This can, presumably, be attributed to the high degree of microstrain and/or sub-micron coherent diffracting domain size arising from the high strain rate impact of powder particles.

Figure 5 shows the open circuit potential (OCP) values of bulk titanium, carbon steel, as-sprayed coating (on carbon steel) and a laser-treated coating (on carbon steel) in aerated solution for 3600 seconds. The OCP of bulk titanium increased steadily over the period of the experiment and reached approximately -285mV from an initial value of -600mV. This change could be due to the growth and establishment of a more protective surface oxide film on the initially as-ground Ti surface when exposed to the test solution [23]. However, the reasons for the noise on the bulk Ti curve are not presently understood but could be due to localized and repeated corrosion events on the surface during the establishment of the more stable oxide. In contrast, the as-sprayed titanium coating had a much lower steady state OCP of about -500mV and remained at that level during the full length of the experiment. The laser-treated titanium coating on the other hand showed a relatively steady OCP which reached about -285mV; the same as that of bulk titanium after 3600 seconds. The fact that it did not increase over time like bulk Ti would suggest it already had a stable oxide film on its surface prior to immersion or that it formed within the first few second of immersion. This could be due to the presence of the TiO phase noted to be present from the XRD pattern of Fig. 4. Therefore, the laser

treatment of the coating shifted the OCP by about -210mV in the more positive direction (i.e. towards the value of bulk titanium) compared to the as-sprayed titanium coating. The steady decrease in the OCP exhibited by bulk carbon steel from -400 to -600mV was indicative of ongoing active corrosion experienced by the ground steel specimen in the test solution. It is also notable that the OCP of the as sprayed coating attained a value between bulk Ti and bulk carbon steel which is indicative of a porous microstructure.

Potentiodynamic polarization scans of bulk titanium, carbon steel, the as-sprayed coating (on carbon steel) and the laser-treated coating (on carbon steel) are shown in Figure 6. Bulk titanium shows a passive current density (I_{pp}) of 0.004mA.cm^{-2} whereas the as-sprayed titanium coating shows only a "passive like" current density of 0.6mA.cm^{-2}, which is two orders of magnitude greater than that of bulk titanium. However, the laser treated coating shows an average I_{pp} of 0.005mA.cm^{-2}, which is virtually the same as the bulk titanium and two orders of magnitude lower than that of the as-sprayed coating. Occasional spikes seen on the anodic polarization curve of the bulk Ti could be due to isolated pitting and re-passivation events as the voltage is increased. In addition, the as-sprayed coating had an I_{corr} value of 5×10^{-3}mA.cm^{-2}; which was reduced to 5×10^{-5}mA.cm^{-2} following laser treatment (Table 4). E_{corr} values of all the samples showed a similar trend to the OCP measurements. A number of small current transients were observed in the bulk Ti scan which may be attributed to metastable pitting during establishment of a more protective surface oxide film on the ground Ti surface.

Figures 7 (a) and (b) show low magnification cross-sections of the as-sprayed coating and laser treated coating respectively after the electrochemical tests in the aerated solution. It is evident that the coating-substrate interface of the as-sprayed sample has severe pitting following the electrochemical tests whereas the laser-treated coating-substrate interface is free from any defect or pitting. Figures 7 (c) and (d) show higher magnification images of the respective coating-substrate interfaces which confirm the severe pitting associated with the as-sprayed coating on carbon steel without the benefit of laser treatment.

3 Discussion

Following laser surface melting, the inter-particle porosity in the top 140µm of the coating was eliminated. In the laser-treated zone the rounded shape of the as-sprayed particles was also

eliminated and an equiaxed grain structure formed upon solidification and cooling to room temperature (Fig. 2). However, the etched microstructure of the coating showed a few isolated submicron-sized pores (Fig. 3-b). These pores are probably trapped gas pores which are typical features in laser-treated, thermal sprayed coatings. Titanium has a high melting temperature (1668°C) and a high affinity for oxygen and nitrogen; it goes through an allotropic phase transformation at 882°C, where hexagonally close packed (hcp) α-titanium transforms to body centered cubic (bcc) β-titanium. On solidification, bcc β-titanium is expected to form from the melt. Cooling in the solid state will give either hcp α-titanium or martensitic α-titanium [21]. It is evident from Fig. 4 that hcp α-titanium has formed. Peak height ratios are as expected from a random, ie not preferentially-oriented α-titanium grain structure. Presumably, columnar β-titanium formed but β- to α-titanium transition gives a random grain orientation. In addition, TiO was detected in XRD spectra of the laser-treated deposit and not TiO_2 (Fig. 4)).

The laser post-treatment of the cold sprayed titanium coating eliminated the interconnected porosity near the surface (Fig. 2) and resulted in a shift of 215mV in the OCP and E_{corr} values towards the noble direction and a decrease, by two orders of magnitude, of the I_{pp} value when compared to the as-sprayed condition. In addition, the OCP did not decrease over time but remained close to the level attained by bulk titanium. Hence, the resolidified top layer provides an impermeable barrier. However, its corrosion characteristics both in terms of OCP and anodic polarization are subtly different to that of bulk titanium. Although post-spray laser treatment has been previously reported to improve the corrosion performance of plasma sprayed titanium coatings [1, 16, 20, 22] further investigation is needed to understand the reasons for the differences in the behavior of bulk and laser treated materials.

Typically, in the presence of an electrolyte at the coating-substrate interface, the carbon steel substrate, being less noble, corrodes and corrosion pits form at the coating-substrate interface; this is clearly seen with the titanium coating tested in the as-sprayed condition (Fig. 7 (a) and (c)). The laser treatment applied following the spray deposition sealed completely the top 150 µm of the coating and pits are not visible as evidenced from Figs. 7 (b) and (d); this occurred as a consequence of the

formation of the melt pool and subsequent solidification which prevents corrosive species from penetrating the coating.

4 Conclusions

Titanium was deposited on carbon steel by cold spraying using nitrogen as a propelling gas. A number of laser trials were performed to eliminate the inter-connected porosity from the top layer of the coatings. The corrosion performance of the as-sprayed and post-spray laser treated coatings were studied in 3.5wt.% NaCl solution. The following conclusions are drawn from the above study:

- Laser surface post-treatment of the cold sprayed titanium coating eliminates interconnected porosity in the top ~140μm of the coatings without any deleterious effect on the substrate.
- The laser-treated titanium coating performs like a high-quality barrier layer and has corrosion values (i.e. OCP, E_{corr} and I_{pp}) very close to those of bulk titanium.

Acknowledgements

The authors would like to thank colleagues at TWI Ltd (Cambridge, UK) and The University of Nottingham (Nottingham, UK) for their service in undertaking this work.

References

[1] T. Kinos, S.L. Chen, P. Siitonen and P. Kettunen, Densification of Plasma Sprayed Titanium and Tantalum Coatings, *J. Thermal Spray Technol.*, 1996, **5(4)**, p 439-444

[2] P.A. Mäusli, Surface Characterisation of Titanium and Titanium alloys, *Advances in Biomaterials*, 1986, **6**, p 57-62

[3] R. Krepski, Thermal Spray Coating Applications in the Chemical Process Industries, M.T.I. Publication No. 42, NACE International, US, 1993.

[4] D.M. Brunette, P. Tengvall et al., Titanium in Medicine: Material Science, Surface Science, Engineering, Biological Responses and Medical Applications, 2001, Berlin, London Springer, p 376-415

[5] E. Muehlberger, Method and Apparatus for Effecting High-Energy Dynamic Coating of Substrates, 1973, PS No 3.839.618: US

[6] T. Schmidt, F. Gärtner and H. Kreye, New Developments in Cold Spray Based on Higher Gas and Particle Temperatures, *J. Thermal Spray Technol.*, **15(4)**, 2006, p 488-494

[7] T. Marrocco, D.G. McCartney, P.H. Shipway and A.J. Sturgeon, Production of Titanium Deposits by Cold-Gas Dynamic Spray: Numerical Modeling and Experimental Characterization, *J. Thermal Spray Technol.*, 2006, **15(2)**, p 263-272

[8] S.H. Zahiri, C.L. Antonio and M. Jahedi, Elimination of Porosity in Directly Fabricated Titanium Via Cold Gas Dynamic Spraying, *J. Mater. Processing Technol.*, 2009, **209(2)**, p 922-929

[9] H.R. Wang, B.R. Hou, J. Wang, Q. Wang and W.Y. Li, Effect of Process Conditions on Microstructure and Corrosion Resistance of Cold-Sprayed Ti Coatings, *J. Thermal Spray Technol.*, 2008, **17(5-6)**, p 736-741

[10] D.L. Gilmore, R.C. Dykhuizen et al., Particle Velocity and Deposition Efficiency in the Cold Spray Process, *J. Thermal Spray Technol.*, 1999, **8(4)**, p 576-582

[11] W.-Y. Li and C.-J. Li, Deposition Characteristics of Titanium Coating in Cold Spraying, *Surface Coat. Technol.*, 2003, 167, p 278-283

[12] T. Hussain, D.G. McCartney, P.H. Shipway and T. Marrocco, Corrosion Behavior of Cold Sprayed Titanium Coatings and Free Standing Deposits, *J. Thermal Spray Technol.*, 2011, **20 (1-2),** p 260- 274

[13] H.R. Wang, W.Y. Li, L. Ma, J. Wang and Q. Wang, Corrosion Behavior of Cold Sprayed Titanium Protective Coating on 1Cr13 Substrate in Seawater, *Surface and Coatings Technology*, 2007, **201(9-11)**: p. 5203-5206

[14] W.-M. Zhao, C. Liu, L.-X. Dong and Y. Wang, Effects of Arc Spray Process Parameters on Corrosion Resistance of Ti Coatings, *J. Thermal Spray Technol.*, 2009. **18(4)**: p. 702-707

[15] K. Ishikawa, T. Suzuki, Y. Kitamura and S. Tobe, Corrosion resistance of thermal sprayed titanium coatings in chloride solution, *J. Thermal Spray Technol.*, 1999, **8(2)**, p 273-278

[16] T. Kinos, S.L. Chen, P. Siitonen and P. Kettunen, Corrosion Properties of Shrouded Plasma Sprayed Titanium Coatings, *Thermal Spraying: Current Status and Future Trends*, A. Ohmori, Ed., 1995, High Temperature Society of Japan (Kobe, Japan), p 573-576

[17] J. Kawakita, H. Katanoda, M. Watanabe, K. Yokoyama and S. Kuroda, Warm Spraying: An Improved Spray Process to Deposit Novel Coatings, *Surface Coat. Technol.*, 2008, **202(18)**, p 4369-4373

[18] W.M. Steen, Laser Material Processing, 3rd edition, 2003, Springer

[19] J.C. Ion, Laser Processing of Engineering Materials: Principles, Procedure and Industrial Application, 2005, Elsevier Butterworth-Heinemann

[20] H.D. Steffens, J. Wilden and C. Buchmann, Laser Beam Nitriding of Thermally Sprayed Titanium Coatings, *Thermal Spraying: Current Status and Future Trends*, A. Ohmori, Ed., 1995, High Temperature Society of Japan (Kobe, Japan), p 981- 986

[21] P. Danielson, R. Wilson and D. Alman, Microstructure of Titanium Welds, *Advanced Materials & Processes*, 2003, **161(2)**, p 39-42

[22] J.D. Ayers, R.J. Schaefer, F.D. Bogar and E. McCafferty, Corrosion Behavior of Laser Consolidated Titanium Coated Steel in Sea-Water, *Corrosion*, 1981, **37(1)**, p 55-57

[23] N. D. Tomashov and P. M. Altovskii, Corrosion and Protection of Titanium, Government Scientific - Technical Publication of Machine-Building Literature (Russian Translation), Moscow, Russia, 1963

Figure 1 (a) Scanning electron micrograph of gas atomized grade 2 titanium feedstock powder. (b) Cumulative size distribution of titanium powder measured by laser diffractometry.

Figure 2 Optical micrographs showing laser-treated areas in titanium coatings, Runs 1-5. All cross-sections were etched prior to microscopy.

Figure 3 (a) Back scattered electron (BSE) image of a laser-treated titanium coating showing the shape of the melt pool and (b) secondary electron (SE) image showing the microstructure of the laser-treated zone. Both cross-sections were taken from the coating treated in Run 3 and etched in Kroll's reagent prior to microscopy. Arrows showing isolated pores.

Figure 4 X-ray diffraction spectra of the as-sprayed and laser-treated titanium coating (Run 3).

Figure 5 Open circuit potential (OCP) in aerated 3.5% NaCl of bulk Ti, carbon steel, as-sprayed Ti coating (on carbon steel) and laser-treated Ti coating.

Figure 6 Potentiodynamic polarization scans in aerated 3.5% NaCl of bulk Ti, carbon steel, as-sprayed Ti coating (on carbon steel) and laser-treated Ti coating.

Figure 7 SE images of unetched coatings: (a) as-sprayed (onto carbon steel) and (b) laser-treated coatings after electrochemical tests. (c) and (d) are the corresponding high magnification images at the interface.

Table 1 Chemical composition and particle size distribution of the titanium powder as supplied by the manufacturer and size distribution measured by laser diffractometry

Table 2 Process parameters used for depositing the titanium coating with the CGT Kinetiks 4000/47® system. P_{GAS} is the gas pressure, GFR is the total nitrogen gas flow rate, PFR is the measured powder feed rate and SOD is the stand-off distance.

Table 3 Process parameters for single track runs in the laser surface treatment of the titanium coatings. Run #3 parameters were employed in the final treatment of the corrosion test samples

Table 4 Corrosion values (in aerated 3.5 wt% NaCl) of bulk titanium, as-sprayed coating (on carbon steel), laser-treated coating and bulk carbon steel.

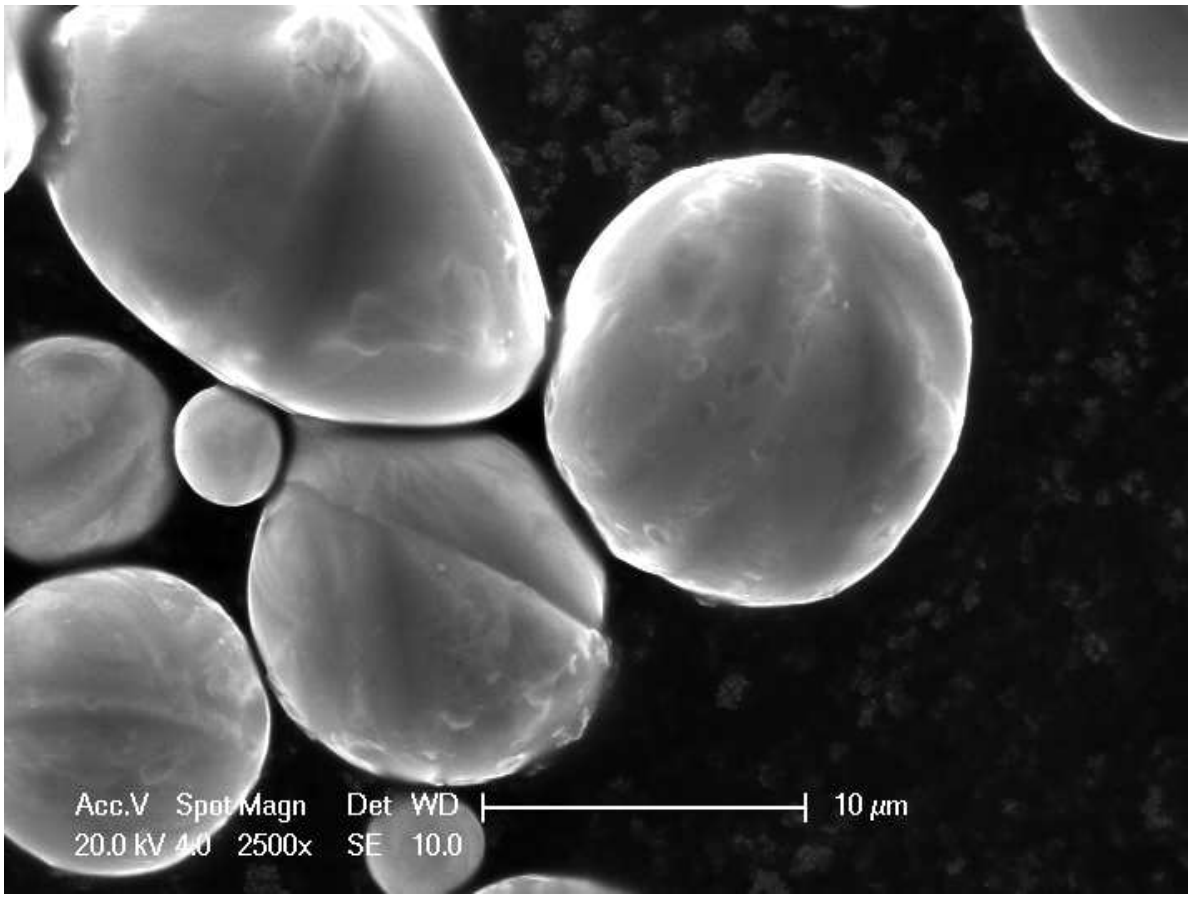
Acc.V Spot Magn Det WD 10 μm
20.0 kV 4.0 2500x SE 10.0

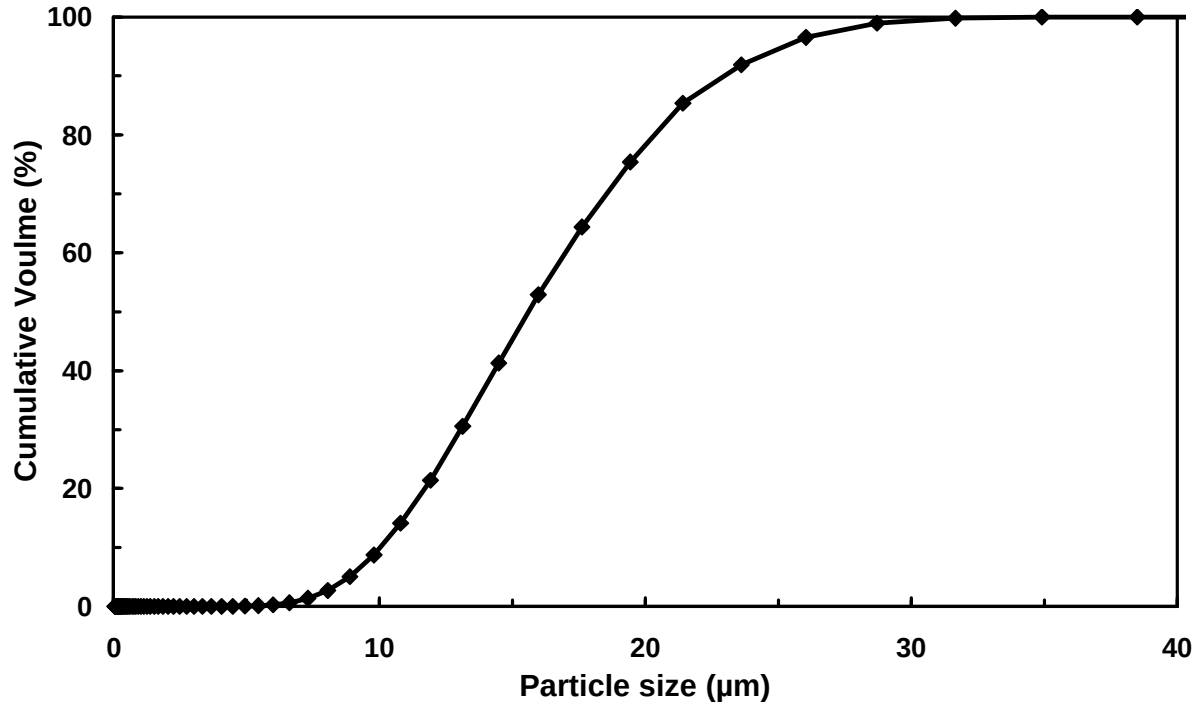
Cumulative Voulme (%)
100
80
60
40
20
0
0
10
20
30
40
Particle size (μm)

Figure 1

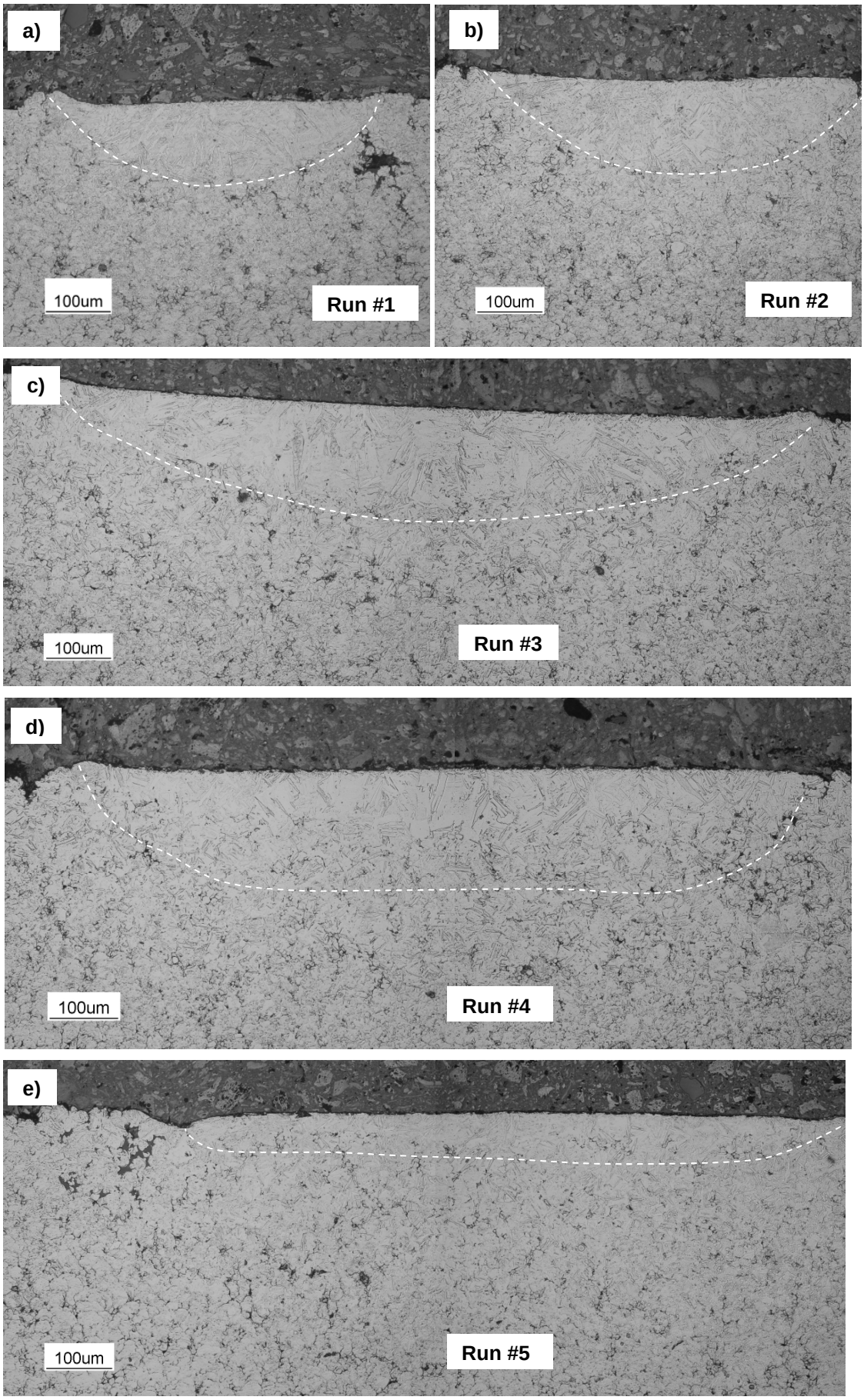
a)
100um
Run #1
b)
100um
Run #2
c)
100um
Run #3
d)
100um
Run #4
e)
100um
Run #5

Figure 2

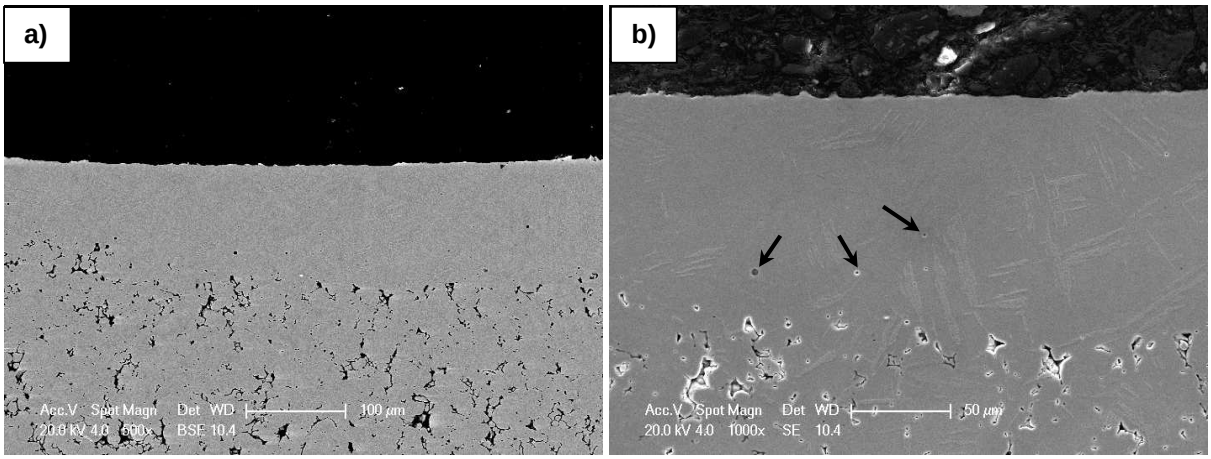

Figure 3

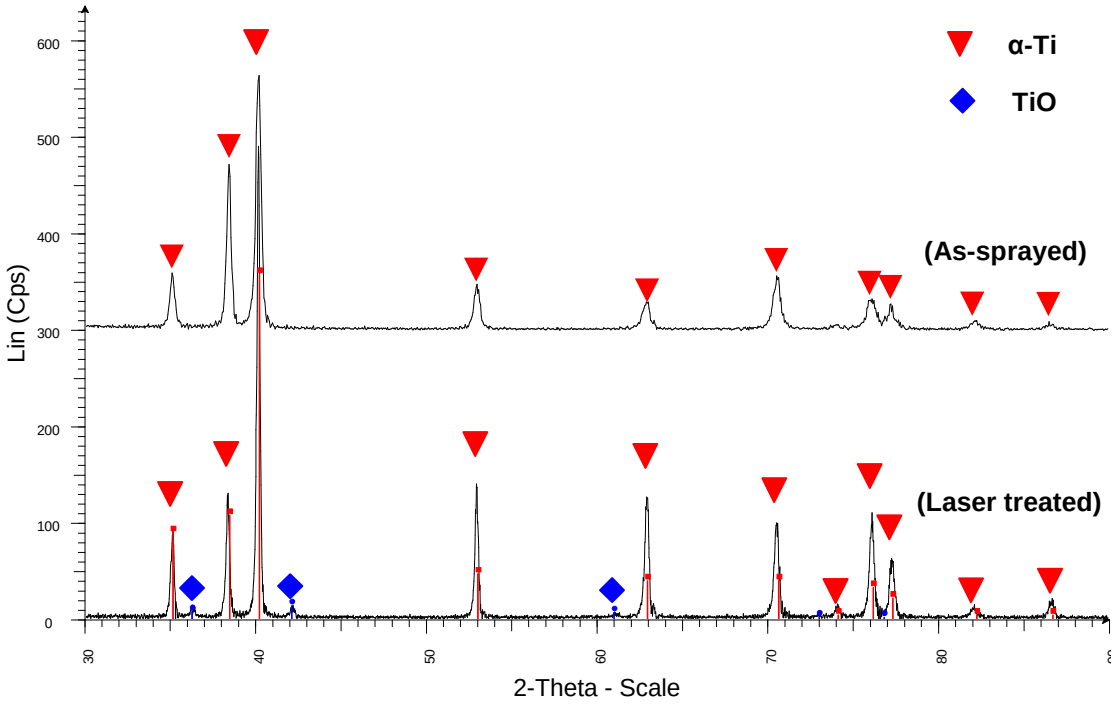

Figure 4

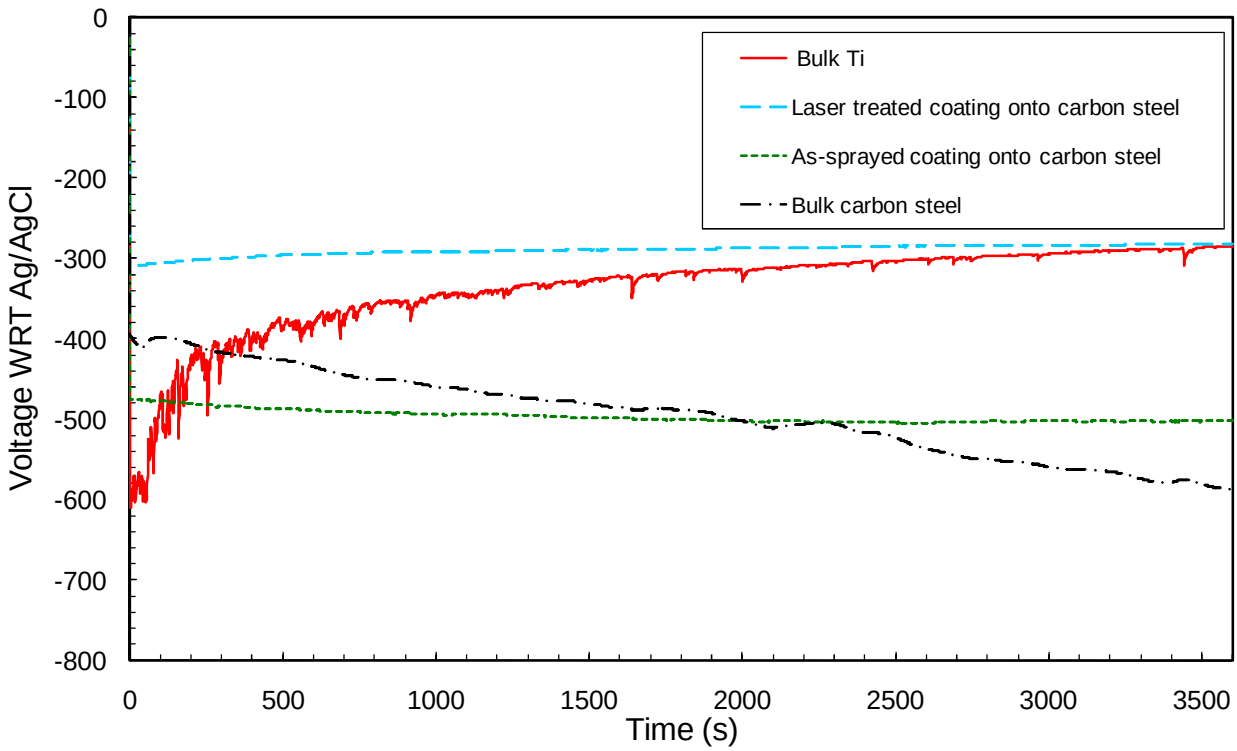

Figure 5

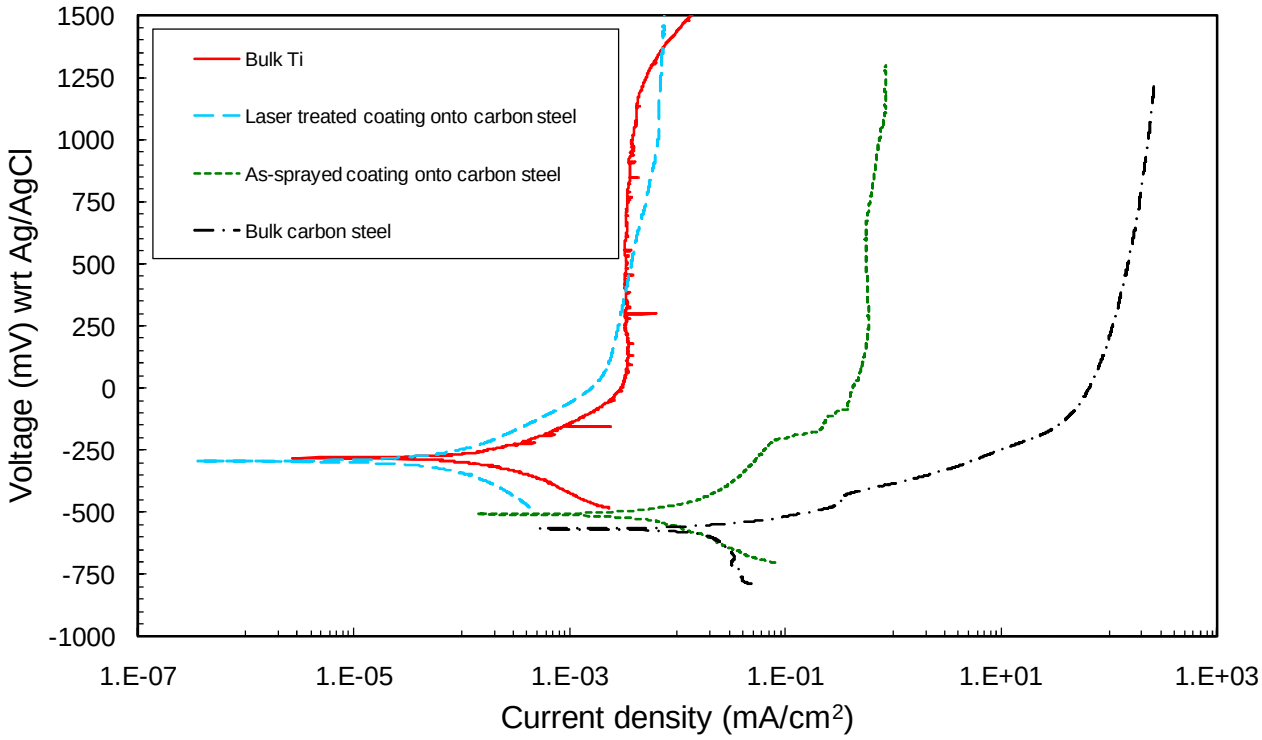

Figure 6

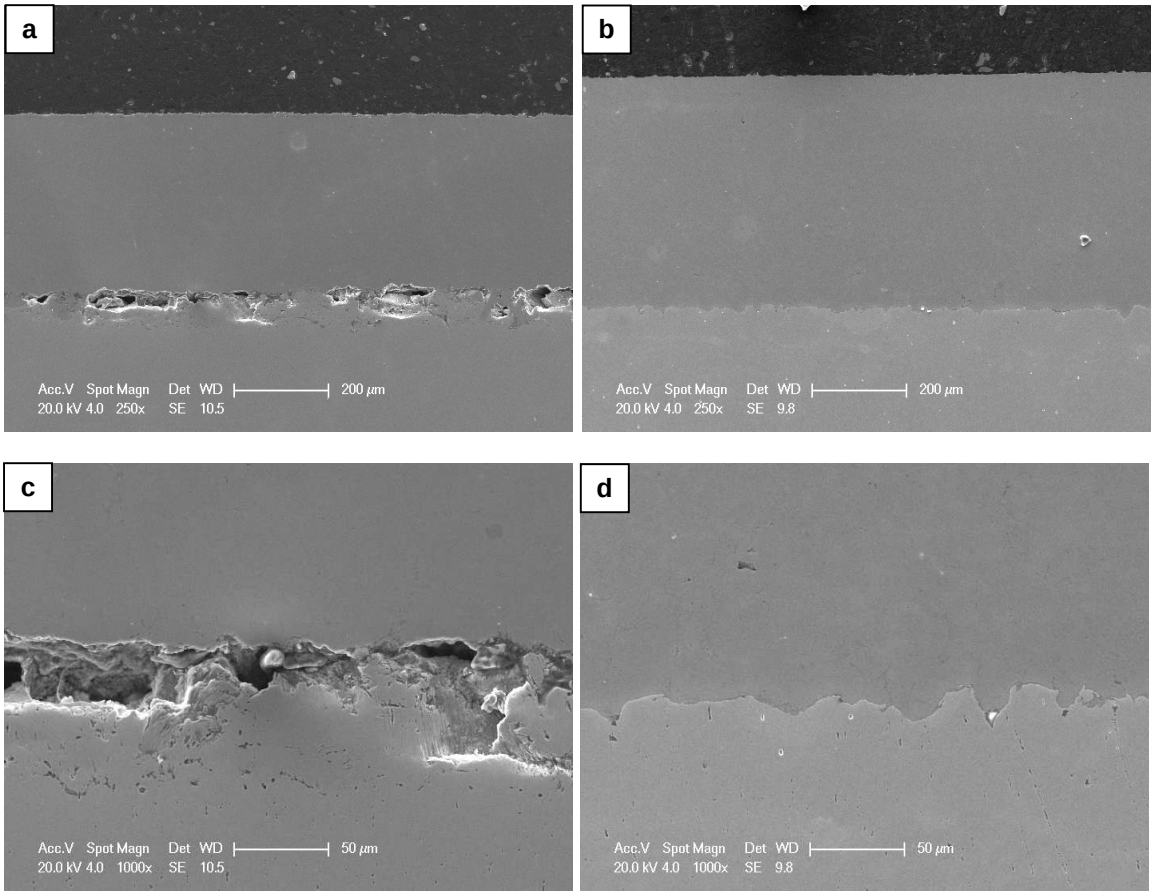
a
Acc.V Spot Magn Det WD 200 µm
20.0 kV 4.0 250x SE 10.5
b
Acc.V Spot Magn Det WD 200 µm
20.0 kV 4.0 250x SE 9.8
c
Acc.V Spot Magn Det WD 50 µm
20.0 kV 4.0 1000x SE 10.5
d
Acc.V Spot Magn Det WD 50 µm
20.0 kV 4.0 1000x SE 9.8

Figure 7

Table 1

Powder	Chemical composition, wt.%					
CP-Ti Grade 2	C	Fe	H	N	O	Ti
	0.008	0.057	0.002	0.002	0.200	Bal.
	Particle size distribution, µm					
				D_{10}	D_{50}	D_{90}
	Supplied			7	16	27
	Measured			10	15	20

Table 2

Process parameter	Set value
P_{GAS}, bar (MPa)	40 (4.0)
GFR, $m^3.h^{-1}$ ($l.min^{-1}$)	80 (1333)
T_{GAS}, °C	800
PFR, $g.min^{-1}$ ($kg.h^{-1}$)	27 (1.6)
SOD, mm	40

NOTE: GFR= Gas flow rate
PFR= Powder feed rate
SOD= Stand-off distance

Table 3

Run No	Power (P), W	Scanning speed (V), $mm.s^{-1}$	Spot size (D), mm	Track (melt) width, μm	Melted depth, μm	$\frac{P}{\sqrt{D \times V}}$, $N.s^{-0.5}$ (E+05)
1	440	25	0.3	500	110	1.61
2	540	25	0.408	600	130	1.69
3	1000	21.6	0.108	1200	140	2.07
4	1000	31.6	0.108	1200	115	1.71
5	1000	48.3	0.108	1200	55	1.38

Table 4

Specimens	OCP, mV [(a)]	E_{corr}, mV [(a)]	I_{corr}, $mA.cm^{-2}$	I_{pp}, $mA.cm^{-2}$
Bulk titanium	-285	-281	1×10^{-4}	0.004
As-sprayed coating (onto carbon steel)	-500	-507	5×10^{-3}	0.6
Laser-treated coating	-285	-294	5×10^{-5}	0.005
Carbon steel	-590	-567	2×10^{-2}	-

[(a)] wrt Ag/AgCl